J|A|C|S
ARTICLES
Published on Web 04/12/2003

Non-Localized Ligand-to-Metal Charge Transfer Excited States in $(Cp)_2Ti(IV)(NCS)_2$

Elizabeth L. Patrick, Chad J. Ray,[†] Grant D. Meyer,[†] Theodore P. Ortiz, Jason A. Marshall, James A. Brozik,* Melissa A. Summers,[†,‡] and John W. Kenney, III*,[§]

Contribution from the Department of Chemistry, The University of New Mexico, Albuquerque, New Mexico 87131, the Department of Chemistry, The Colorado College, Colorado Springs, Colorado 80903, and the Chemical Physics Laboratory, Division of Natural Science, Concordia University—Irvine, Irvine, California 92612

Received October 2, 2002; E-mail: brozik@unm.edu; John.Kenney@cui.edu

Abstract: The bent d^0 titanium metallocene $(Cp)_2Ti(NCS)_2$ exhibits an intense phosphorescence from a ligand-to-metal charge transfer triplet excited state at 77 K in an organic glass substrate and a poly(methyl methacrylate) plastic substrate. Quantum chemical calculations and spectroscopic studies show that the orbital parentage of this triplet state arises from the promotion of an electron from an essentially nonbonding symmetry adapted π molecular orbital located on the NCS^- ligands to a $d_{z^2-y^2}$ orbital located on the Ti metal. Standard infrared spectroscopy of $(Cp)_2Ti(NCS)_2$ in its ground electronic state at 77 K reveals a pair of closely spaced absorptions at $(2072\ cm^{-1}, 2038\ cm^{-1})_{glass}$ and $(2055\ cm^{-1}, 2015\ cm^{-1})_{plastic}$ that are assigned, respectively, to the symmetric and antisymmetric CN stretching modes of the two coordinated NCS^- ligands. Low-temperature (77 K) time-resolved infrared spectroscopy that accesses the phosphorescing triplet excited state on the ns time scale shows an IR bleach that is coincident with the two ground state CN stretching bands and an associated grow-in of a pair of new IR bands at slightly lower energies $(2059\ cm^{-1}, 2013\ cm^{-1})_{glass}$ and $(2049\ cm^{-1}, 1996\ cm^{-1})_{plastic}$ that are assigned, respectively, to the symmetric and antisymmetric CN stretches in the emitting triplet state. These transient IR bands decay with virtually identical lifetimes to those observed for the phosphorescence decays when measured under identical experimental conditions. Singular value decomposition analysis of the time-resolved infrared data shows that the observed transient IR features arise from the same electronic manifold as measured through luminescence studies. The close similarity between the ground state and excited-state CN stretching bands in $(Cp)_2Ti(NCS)_2$ indicates that symmetry breaking does not occur in forming the charge-transfer triplet excited-state manifold; i.e., electron density is withdrawn from a delocalized π MO spread across both NCS^- ligands. Calculations at several levels of theory reveal a delocalized ligand-to-metal charge transfer excited triplet manifold. These calculations closely reproduce the relative intensity ratios and frequencies of the symmetric and antisymmetric transient infrared vibrations in the CN region. This study is the first time-resolved infrared investigation of a ligand-to-metal charge-transfer excited state and the first to be performed at cryogenic temperatures in thin-film organic glass and plastic substrates.

I. Introduction

One of the major problems surrounding the study of bent $(Cp)_2M(IV)X_2$ metallocenes (where M(IV) = Ti(IV), Zr(IV) or Hf(IV) and Cp = cyclopentadienyl (η^5-C_5H_5) and X = halide or pseudo-halide) is the identification and correct orbital assignment of their lowest energy excited electronic states.[1] Because the metal centers of this family of metallocenes are formally d^0 in almost all cases, the lowest excited states are ligand-to-metal charge transfer (LMCT) in nature. The ambiguity arises because the highest occupied molecular orbitals (HOMOs) in this class of materials—whether they are located on the Cp rings, the halides, or the pseudo-halides—are all very close in energy and can give rise to a number of close-lying excited states. In addition, the lowest emitting states in molecules containing transition metals are often spin triplets that give rise to spin forbidden phosphorescence emissions into a ground singlet state. Spin−orbit coupling can split these triplets into three separate states, each with distinct energetic, decay, and symmetry properties. In these cases, excited-state assignments based upon simple one-electron promotions (e.g., a HOMO → lowest unoccupied molecular orbital (LUMO) promotion) are either not very reliable or miss important details. Thus, one

[†] Present Addresses: Melissa A. Summers, Department of Chemistry & Biochemistry, University of California, Santa Barbara, Santa Barbara, CA 93106. Chad J. Ray, P. M. Gross Chemistry Laboratory, Duke University, Box 90348, Durham, NC 27708-0348. Grant D. Meyer, Biomedical Engineering Program, Cornell University, Olin Hall, Ithaca, NY 14850.
[‡] Department of Chemistry, The Colorado College.
[§] Chemical Physics Laboratory, Division of Natural Science, Concordia University—Irvine.

(1) Kenney, J. W., III.; Boone, D. R.; Striplin, D. R.; Chen, Y.-H.; Hamar, K. B. *Organometallics* **1993**, *12*, 3671−3676.

needs to appeal to experiment and higher-level excited-state calculations to determine the true orbital nature of the lowest excited states.

A second issue involving transition metal complexes and organometallic compounds (that possess a center of symmetry) has been that of electronic localization after optical excitation. It has been shown over the years that in most (if not all) cases involving triplet metal-to-ligand charge transfer (^{3}MLCT) excited electronic states, that optical excitation results in the promotion of an electron from the metal to only one peripheral ligand (often described as a symmetry broken excited state). The mechanism for this symmetry breaking is still not well understood and is an active area of research.[2−4] The classic example of such a ligand-localized ^{3}MLCT excited state in a transition metal complex is that observed in $[Ru(bpy)_3]^{2+}$ for which it is well established that the $d_M \rightarrow \pi_{bpy}$ MLCT electron promotion transfers electron density to only one of the three bpy ligands.[5−10] For molecules with ^{3}LMCT states such as the $(Cp)_2M(IV)\ X_2$ metallocenes, a similar question must be asked. Does the "hole" arising from the $\pi_{Cp\ or\ X} \rightarrow d_M$ LMCT electronic excitation reside on only one ligand (only one Cp ring or one X) or is it delocalized over the entire symmetry adapted set of equivalent ligands (both Cp rings or both X ligands)? Because the electronic nature of a ^{3}LMCT state is fundamentally different from that of a ^{3}MLCT state (the ligands are oxidized rather than reduced) there is no inherent reason to expect that the ligand-localized excited electron behavior seen in ^{3}MLCT excited states should carry over to a corresponding ligand-localized hole behavior in ^{3}LMCT states. This issue has never been addressed for molecules with low-lying ^{3}LMCT states, perhaps because there are so few examples of molecules with ^{3}LMCT excited states that are long-lived enough and have suitable symmetries for such studies.

This study addresses, in detail, the orbital nature of the lowest emitting triplet manifold in $(Cp)_2Ti(NCS)_2$ as well as the symmetry (and thus the extent of delocalization) of this ^{3}LMCT state in comparison to the symmetry of the singlet ground state. All spectral evidence points to a nonlocalized $\pi_{NCS} \rightarrow d_{Ti}$ ^{3}LMCT assignment for the emissive state. This assignment is corroborated by quantum chemical calculations. This work is unique in that it is the first time-resolved infrared (TRIR) study of a ^{3}LMCT state and the first to be conducted at 77 K in organic glasses and plastic films. Many of the nuances of the luminescence and TRIR data interpretation are extracted from statistical analyses and quantum chemical modeling studies of the ground and several low-lying ^{1}LMCT and ^{3}LMCT excited states of this system.

II. Experimental

(A) Synthesis and Materials. The chemical synthesis of $(Cp)_2Ti(NCS)_2$ was adapted from the work of Giddings et al.[11] Because of the occurrence of a very small, but measurable amount of an oxygen-bridged dimer when the synthesis was performed in air,[11] all procedures were performed under inert atmosphere and dry conditions. Reagent grade acetone was purchased from EM Science and distilled and degassed (three consecutive freeze−pump−thaw cycles) prior to use. $(Cp)_2TiCl_2$ and KSCN were purchased from Aldrich Chemical company and used as received. All manipulations of chemicals and reaction vessels were performed inside a glovebox and the reactions were carried out on a standard Schlenk line under an argon atmosphere. The preparation and purification of $(Cp)_2Ti(NCS)_2$ was carried out as follows. 24.9 mg (0.1 mmol) of $(Cp)_2TiCl_2$ and 9.7 mg (0.2 mmol) of KSCN were placed in a 4-mL reaction vial with a condenser attachment. The reaction vessel was attached to a Schlenk line, and 1 mL of acetone was transferred to the reaction vial via a syringe. The mixture was then heated to reflux for 2 h while being continually stirred. After cooling to room temperature, a dark red solution resulted, and a white precipitate formed. The white precipitate (KCl) was removed from the solution by suction filtration inside a glovebox. The resultant solution was then placed in a sealed jar surrounded by a small amount of diethyl ether. The jar was sealed from air and placed in a refrigerator overnight, upon which large, well-formed crystals of $(Cp)_2Ti(NCS)_2$ were obtained. X-ray crystallography and elemental analysis were used to verify the nature of the final product. X-ray and IR data on the crystals matched previously published results.[12−14] Desert Analytics performed the elemental analysis and the results are as follows: (theoretical; 16.27% Ti, 21.80% S, 9.52% N, 48.99% C, 3.43% H: experimental; 16.03% Ti, 21.79% S, 9.56% N, 49.01% C, 3.51% H).

(B) Spectroscopic Sample Preparation. All solvents were reagent grade (purchased from EM Science) and freshly distilled and degassed prior to use. Poly(methyl methacrylate) (PMMA) was purchased from Aldrich Chemical Co., had a molecular weight of ∼120 000 and was used as received. Samples for spectroscopic study were prepared as thin films of PMMA or as a thin organic glass of 3:2:1 $CHCl_3$:CCl_4:CH_2Cl_2. Solutions for the preparation of PMMA films were prepared by dissolving ∼1 mg of $(Cp)_2Ti(NCS)_2$ and 50 mg of PMMA in CH_2Cl_2. The exact concentration of $(Cp)_2Ti(NCS)_2$ in PMMA was adjusted so that the thin films of PMMA had an average maximum IR absorbance of ∼0.5 at 2015 cm^{-1} and 77 K (room-temperature absorbance at 532 nm was ∼0.1). For 77 K steady-state emission, luminescence lifetimes and time-resolved IR experiments, thin films of PMMA were prepared by casting the $(Cp)_2Ti(NCS)_2$/PMMA/CH_2Cl_2 solution in shallow aluminum molds and allowing them to dry (∼24 h) under an argon atmosphere. The resultant thin films, which were peeled from their aluminum molds after drying for spectroscopic study, had an average thickness of 90 μm. Although the above-mentioned method for producing thin films is appropriate for the experiments listed, it was not suitable for ground electronic state FTIR experiments in which the samples and reference backgrounds needed to be the same thickness. Therefore, PMMA samples and blanks for ground-state FTIR experiments were prepared by spin coating them onto CaF_2 optical flats with a spin coater (Headway Inc. Model 1-EC101D-R790). During the spin coating process, the samples were exposed to air. Because these films were much thinner than the delaminated films described above, the optical absorbance at 2015 cm^{-1} was considerably smaller.

Thin organic glasses were prepared by adjusting the concentration of $(Cp)_2Ti(NCS)_2$ in 3:2:1 $CHCl_3$:CCl_4:CH_2Cl_2 until the average IR absorbance was ∼0.5 at 2038 cm^{-1} and 77 K (room-temperature absorbance at 532 nm was ∼0.08). Inside a glovebag purged with dry nitrogen, a thin film (like a soap bubble) of the sample solution was spread across a 3-mm hole drilled into a custom-made bronze sample holder that was subsequently attached to the thermal base of a 77 K

(2) Yeh, A. T.; Shank, C. V.; McCusker, J. K. *Science* **2000**, *289*, 935−938.
(3) Damrauer, N. H.; Weldon, B. T.; McCusker, J. K. *J. Phys. Chem. A* **1998**, *103*, 3382−3397.
(4) Damrauer, N. H.; Cerullo, G.; Yeh, A. T.; Boussie, T. R.; Shank, C. V.; McCusker, J. K. *Science* **1997**, *275*, 54−57.
(5) Bradley, P. G.; Kress, N.; Hornberger, B. A.; Dallinger, R. F.; Woodruff, W. H. *J. Am. Chem. Soc.* **1981**, *103*, 7441−7446.
(6) Forster, M.; Hester, R. E. *Chem. Phys. Lett.* **1981**, *81*, 42−47.
(7) Gold, J. S.; Milder, S. J.; Lewis, J. W.; Kliger, D. S. *J. Am. Chem. Soc.* **1985**, *107*, 8285−8286.
(8) Brus, L. E.; Carroll, P. J. *J. Am. Chem. Soc.* **1987**, *109*, 7613−7616.
(9) Kober, E. M.; Sullivan, B. P.; Meyer, T. J. *Inorg. Chem.* **1983**, *23*, 2098−2104.
(10) Riesen, H.; Wallace, L.; Krausz, E. *Inorg. Chem.* **1996**, *35*, 6908−6909.
(11) Giddings, S. A. *Inorg. Chem.* **1967**, *6*, 849−850.
(12) Villa, A. C.; Manfredotti, A. G.; Guastini, C. *Acta Crystallogr.* **1976**, *B32*, 909−914.
(13) Coutts, R. S. P.; Wailes, P. C. *Aust. J. Chem.* **1966**, *19*, 2069−2072.
(14) Burmeister, J. L.; Deardorff, E. A.; Dyke, C. V. *Inorg. Chem.* **1969**, *8*, 170−172.

cryostat (Janis Inc., model VPF-100). An organic glass was made by flash freezing the sample in a dewar of liquid nitrogen. The cryostat was then filled with liquid nitrogen, assembled, a vacuum was pulled on the frozen glass and the cryostat was removed from the glovebag.

(C) Steady-State Emission. Steady-state emission spectra of $(Cp)_2Ti(NCS)_2$ samples were obtained from samples mounted onto a brass sample holder attached to the coldfinger of a cryostat and cooled to 77 K (as described above). The cryostat was equipped with CaF_2 windows for both luminescence and IR experiments. The temperature was monitored with a silicon diode calibrated between 1.4 and 325 K (Lake Shore Cryotronics Inc., model DT-470-SC-13−1.4L) and controlled with a temperature controller (Lake Shore Cryotronics Inc., model 330). The excitation source was the doubled output of a cw-Nd:YAG laser that produced a 20 mW 532 nm line (BWTEK Inc.). The laser was passed through an Opto-Sigma 532 nm laser line filter, attenuated to 3 mW by a series of neutral density filters and aimed directly onto the sample. Emitted light was monitored at 90° to the excitation beam, filtered through a low pass glass filter (Schott Glass OG-550), dispersed by an Acton 500i monochromator, and detected by a thermoelectrically cooled Hamamatsu R943−02 photomultiplier. The detector signal was passed through a wide-band preamplifier and fed to a Stanford Research Systems SR400 photon counter. Data were transferred to a PC for further manipulations. All spectra were corrected against a quartz tungsten halogen spectral irradiance standard lamp (Oriel Inc.).

(D) Luminescence Lifetimes. For luminescence decay-time measurements at 77 K, the sample preparation method and detection system were as described above. The excitation source was the doubled output of a Continuum Minilite Nd:YAG (532 nm, 4 ns pulse width, 1 mJ pulse energy) laser. An optical trigger synchronized the photon counter to the pulse train. The data were transferred to a PC for further analysis. All data reduction was achieved by means of a curve-fitting program (IGOR, Wavemetrics Inc.).

(E) Low-Temperature FTIR. FT-IR spectra were measured with a Nicolet Nexus 870 FTIR spectrophotometer. Both glass and plastic samples were mounted in a cryostat and cooled to 77 K as described above. The cryostat was mounted directly into the sample compartment of the spectrophotometer via a custom-made mounting plate and aligned with a mechanical stage. All spectra were recorded at 8 cm^{-1} resolution with a liquid nitrogen cooled MCT detector. PMMA plastics have a clear IR window from 2828 to 1760 cm^{-1}, whereas 3:2:1 $CHCl_3$:CCl_4:CH_2Cl_2 has a clear IR window from 2290 to 1600 cm^{-1}.

(F) Time-Resolved IR Spectroscopy at 77 K. Time-resolved IR spectroscopy (TRIR) on the nanosecond time scale was achieved with a step-scan Fourier transform (SS−FTIR) technique. A detailed schematic diagram of the experimental setup is depicted in the Supporting Information (figure S1). In this experiment samples were prepared, mounted, and cooled to 77 K in the Janis cryostat as described above. The entire TRIR spectroscopic experiment is sealed around the cryostat and purged with a continual stream of dry N_2. Electronic excitation is achieved by the doubled output of a Continuum Minilite Nd:YAG (532 nm, 4 ns pulse width, 1 mJ pulse energies) laser and transient IR signatures are probed with a commercial SS−FTIR (Nicolet Nexus 870). Care was taken to overlap the excitation pulse with the IR probe (3 mm diameter). The spectral range of the IR probe is limited by a Janos F1305L300 long pass filter and the CaF_2 windows of the Janis cryostat (spectral range: 3200 cm^{-1} to 1111 cm^{-1}). Timing between the interferometer and the laser is achieved with an optical trigger (photodiode, ThorLabs model DET210) and the entire time domain is recorded with a 100 MHz digital oscilloscope (Gage, model 12100−1M). In SS−FTIR spectroscopy the moveable mirror of the interferometer is moved stepwise (1.264 μm steps in the present study). This mirror was then held stationary at each fixed mirror position while the data was collected. Two sets of data were acquired after each mirror step; one from the AC-coupled output of the MCT detector and the other from its DC-coupled output. The DC signal was collected before the laser was fired and, after a Fourier transform, constituted the single beam static background spectrum. The AC signal was synchronized to the pulse train of the laser and, after a Fourier transform of each time slice, constituted the dynamic time-resolved IR spectral profile recorded at several (up to 25) time delays after each laser pulse. The static spectrum was collected as a time average (250 ms) at each mirror position and the dynamic spectra were collected as a numerical average of 75 laser pulses at each mirror position. The dynamic interferogram at each time delay was obtained by the manipulation of the full array of kinetic data vs mirror position (volts vs mirror position vs time). All time-resolved spectra are plotted in units of change in absorbance (ΔA), which is calculated as $\Delta A = \log(1 + \text{dyamic/static})$ (where dynamic = dynamic single beam spectrum and static = static single beam spectrum).[15] All spectra reported are an average of five individual experiments. Since there is no time limit to the FT method, the time resolution is set by the duration of the laser pulse, the detector time response, the electronic time delay introduced by the optical trigger and the bandwidth of the digitizer. Presently this is on the order of 25 ns in our laboratory and is limited by our optical trigger.

(G) Electronic and Frequency Calculations. All theoretical studies employed Gaussian 98W version 5.2 revision A.7 software[16] which was implemented on a custom built PC with Microsoft Windows 98 as its operating system. The PC was equipped with a 1.6 GHz microprocessor (AMD Athlon XP 1900+), 512 MB of RAM (Corsair PC2400 Cas2 DDR SDRAM) and a 17 GB SCSI hard drive (Seagate 318452LW). The maximum computing time for any one calculation was 5 days but most took about 6 h.

MO diagrams and ground-state vibrational frequencies (IR spectra) were generated using Hartee-Fock (HF) and Density Functional Theories (DFT). Several basis sets were also used including standard Gaussian basis sets (3-21G and 6-31G), a basis set with an electron core potential (LANL2DZ) and basis sets with polarizing functions (6−31g* and 6−31g**).

This present study has also utilized two relatively recent developments for modeling excited electronic states to yield more accurate predictions of excited-state properties and for developing more accurate state diagrams. The first method, Configuration Interaction with Single Substitution or CIS, capitalizes on the HOMO−LUMO concept but expands it by considering a number of excited-state configurations (single electron promotions only) in an iterative procedure until the lowest energies for the number of desired excited states are determined.[17] By allowing the excited states to interact with one another, electron correlation is inherently present and this naturally improves the overall quality of the excited-state energies and properties.

The second method utilized in this study was Time-Dependent Density Functional Theory or TD−DFT. TD methods follow from the general development and derivation of the Random Phase Approximation to describe the evolution of time dependent properties.[18−20] When used to model the excited states of molecules the time dependent property is the response of the ground-state wave function to a time-dependent external electric field (polarization propagator, PP). The poles

(15) Chen, P.; Palmer, R. A. *Appl. Spectrosc.* **1997**, *51*, 580−583.
(16) Frisch, M. J.; Trucks, G. W.; Schlegel, H. B.; Scuseria, G. E.; Robb, M. A.; Cheeseman, J. R.; Zakrzewski, V. G.; Montgomery, J. A., Jr.; Stratmann, R. E.; Burant, J. C.; Dapprich, S.; Millam, J. M.; Daniels, A. D.; Kudin, K. N.; Strain, M. C.; Farkas, O.; Tomasi, J.; Barone, V.; Cossi, M.; Cammi, R.; Mennucci, B.; Pomelli, C.; Adamo, C.; Clifford, S.; Ochterski, J.; Petersson, G. A.; Ayala, P. Y.; Cui, Q.; Morokuma, K.; Salvador, P.; Dannenberg, J. J.; Malick, D. K.; Rabuck, A. D.; Raghavachari, K.; Foresman, J. B.; Cioslowski, J.; Ortiz, J. V.; Baboul, A. G.; Stefanov, B. B.; Liu, G.; Liashenko, A.; Piskorz, P.; Komaromi, I.; Gomperts, R.; Martin, R. L.; Fox, D. J.; Keith, T.; Al-Laham, M. A.; Peng, C. Y.; Nanayakkara, A.; Challacombe, M.; Gill, P. M. W.; Johnson, B.; Chen, W.; Wong, M. W.; Andres, J. L.; Gonzalez, C.; Head-Gordon, M.; Replogle, E. S.; Pople, J. A.; *Gaussian*, revision A.7 ed.; Gaussian: Pittsburgh, PA, 2001.
(17) Foresman, J. B.; Head-Gordon, M.; Pople, J. A.; Frisch, M. J. *J. Phys. Chem.* **1992**, *96*, 135−149.
(18) Oddershede, J. *Adv. Chem. Phys.* **1987**, *69*, 201−239.
(19) Bauernschmitt, R.; Ahlrichs, R. *Chem. Phys. Lett.* **1996**, *256*, 454−464.
(20) Casida, M. E.; Jamorski, C.; Casida, K. C.; Salahub, D. R. *J. Chem. Phys.* **1998**, *108*, 4439−4449.

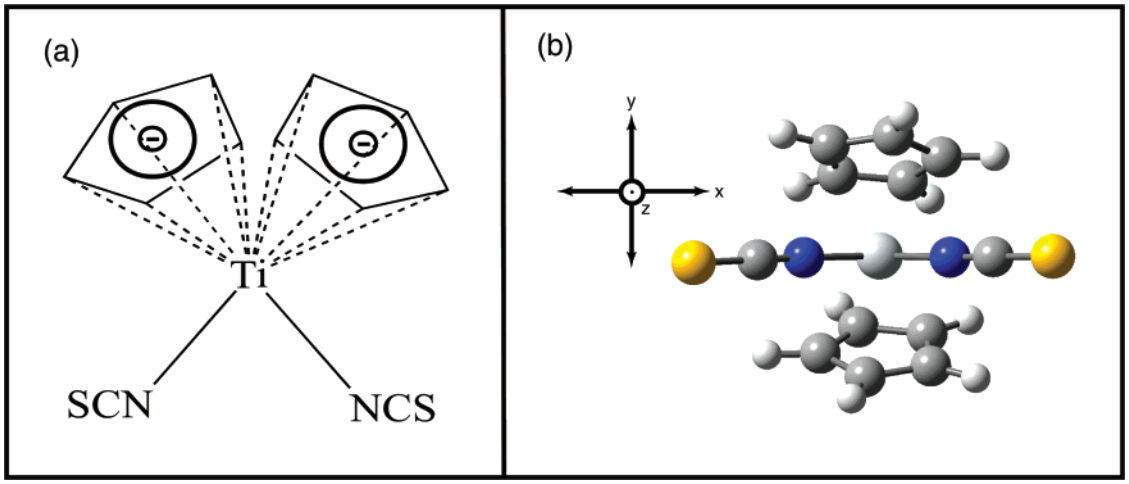

Figure 1. (a) Molecular structure of $(Cp)_2Ti(NCS)_2$ and (b) coordinate system used in the theoretical study.

of the PP (the maximum and minimum range on which the perturbation is valid) are determined by the predicted electron affinity and ionization potential based upon the ground-state calculation.

When performing HF or DFT geometry optimizations the SCF energy is minimized with respect to the 3N nuclear coordinates X_1, Y_1, Z_1, X_2, Y_2, Z_2, ..., X_n, Y_n, Z_n (or in short hand notation R_i ($i = 1, 2, ..., 3N$)) such that

$$f_i = \frac{\partial E}{\partial R_i} = 0 \text{ at the equilibrium geometry}$$

When the SCF energy of the system has been minimized the equilibrium force constants for the 3N-6 vibrational frequencies can be calculated by[21]

$$f_{ij} = \frac{\partial^2 E}{\partial R_i \partial R_j}$$

Moreover, the IR absorption intensities corresponding to each vibrational frequency are proportional to the square of the change in dipole moment with respect to nuclear geometry

$$\text{IR intensity} \propto \left(\frac{\partial \mu}{\partial R}\right)^2 \propto \left(\frac{\partial^2 E}{\partial R \partial F}\right)$$

Where μ is the dipole-moment and F is an external electric field. In this way, one can simulate IR spectra of molecules in their ground electronic state by utilizing the results of HF or DFT calculations.[21,22] Likewise, one can also perform the same analysis for excited state frequency calculations when utilizing the CIS technique. But because TD−DFT uses a polarization propagator to calculate the energies of the excited states, there is currently no *general* way (that the authors are aware of) to perform excited-state frequency calculations using the time-dependent technique. In the present work, ground and excited states frequencies were modeled as described above. In addition all reported frequencies were calculated utilizing basis sets with polarizing functions and then corrected with published frequency correction factors.[22−24] Excited-state IR spectra generated using the CIS method were also corrected in the same manner as the ground-state spectra.[17]

The general molecular geometry used in the quantum chemical modeling study is depicted in Figure 1 in which the C_2 axis comes out of the plane of the paper (Figure 1b).

The geometry chosen has strict C_2 symmetry with the Cp rings staggered in relation to one another. The separate Cp rings and NCS^- ligands are related by a C_2 symmetry operation. This is different from what is measured in the X-ray crystal structure in which the molecule has strict C_{2v} symmetry and the Cp rings are eclipsed. The reason for reducing the symmetry is 2-fold. First, since the Cp rings are nearly free to rotate in solution (crystalline forces lock the Cp rings into the eclipsed position), then it is most likely that there exists a weighted average of all possible Cp conformations trapped in the plastics and glasses. Second, because the most heavily weighted population in organic glasses and PMMA plastics is most probably the lowest energy conformation, we have chosen the staggered geometry as the one that will most accurately model our experimental data. The assertion that the lowest energy structure is the staggered conformation is backed up in all of our calculations. Therefore, the procedure for arriving at a ground state geometry was to start with the crystal structure data, rotate one of the Cp rings such that it is in a staggered position, and then perform a geometry optimization. This was done for each level of theory and basis set. The calculated results and a comparison to a variety of experimentally observed (X-ray data) bond angles and lengths are summarized in table S1 of the Supporting Information. All geometries yielded lower SCF energies than their eclipsed counterparts and none produced imaginary frequencies during ground-state vibrational calculations, whereas the eclipsed geometry did give rise to imaginary vibrational frequencies. Because the spectroscopic experiments were all performed at 77 K in solid matrixes and geometric relaxation of excited-state molecules will be some what hindered by the solid matrix surrounding each molecule, all excited-state calculations have been performed with the optimized ground-state geometries. As expected, each excited-state frequency calculation produced six imaginary frequencies indicating that the geometry was not in an excited-state geometric minimum.

III. Results

(A) Emission Spectra. $(Cp)_2Ti(NCS)_2$ is highly luminescent in low temperature PMMA plastics, organic glasses and in the solid state (crystals). The relative quantum efficiency for luminescence is highly sensitive to the external environment. We observe that $(Cp)_2Ti(NCS)_2$ exhibits a considerably higher relative quantum efficiency for phosphorescence in organic glasses over PMMA plastics and is nearly nonluminescent in room temperature solutions, plastics and in the solid state. Because relative quantum yield experiments are very difficult to quantify for samples prepared as thin organic glasses or plastic films and measured at 77 K, we must note that we are merely

(21) Pople, J. A.; Schlegel, H. B.; Krishnan, R.; Defrees, D. J.; Binkley, J. S.; Frisch, M. J.; Whiteside, R. A. *Int. J. Quantum Chem.: Quantum Chem. Symp.* **1981**, *15*, 269−278.
(22) Wong, M. W. *Chem. Phys. Lett.* **1996**, *256*, 391−399.
(23) Pople, J. A.; Scott, A. P.; Wong, M. W.; Radom, L. *Israel J. Chem.* **1993**, *33*, 345−350.
(24) Scott, A. P.; Radom, L. *J. Phys. Chem.* **1996**, *100*, 16 502−16 513.

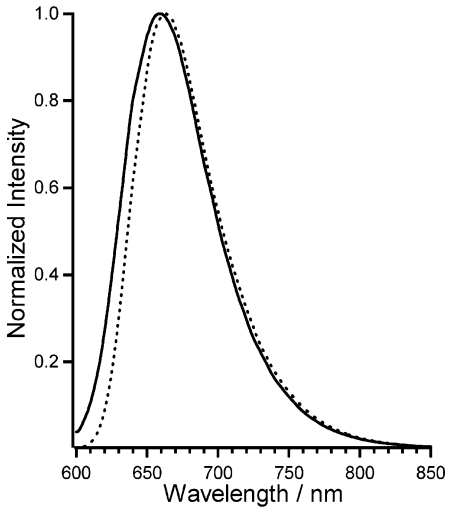

Figure 2. Steady-state emission spectra of $(Cp)_2Ti(NCS)_2$ at 77 K in PMMA (—) and 3:2:1 $CHCl_3$:CCl_4:CH_2Cl_2 (- - -). Samples excited with a 532 nm Nd:YAG laser (3 mW, cw).

Table 1. Luminescence Lifetimes[a]

matrix	$\tau_{lum,\ <10\mu J}$ (μs)	$\tau_{lum,\ 1mJ}$ (μs)	$\tau_{TRIR,\ 1mJ}$ (μs)
PMMA plastic	373	79.4	79.9
$CHCl_3$:CCl_4:CH_2Cl_2 glass	653	589	585

[a] Measured at 77 K measured with the double output of a Nd:YAG laser focused to a 3 mm spot size ($\tau_{lum,\ <10\mu J}$ = luminescence lifetime, excitation pulses <10 μJ; $\tau_{lum,\ 1mJ}$ = luminescence lifetime, 1 mJ excitation pulses). No local heating was observed with pulse energies <10 μJ. TRIR decay transients were calculated from SVD analyses ($\tau_{TRIR,\ 1mJ}$ = decay of transient IR signature, 1 mJ excitation pulses).

reporting a general observation that under the conditions of our 77 K luminescence experiments, the samples prepared as organic glasses have considerably larger luminescence intensities than those prepared in PMMA plastics. Shown in Figure 2 are normalized 77 K luminescence spectra of $(Cp)_2Ti(NCS)_2$ in a PMMA plastic film and a 3:2:1 $CHCl_3$:CCl_4:CH_2Cl_2 organic glass.

These PMMA and organic glass spectra consist of a single broad, structureless, long-lived luminescence band, typical for this class of molecules,[1] that we have assigned to a ^{3}LMCT → ^{1}ground state (^{1}GS) phosphorescence. The orbital character of the phosphorescent ^{3}LMCT manifold arises from a $\pi_{NCS} \rightarrow 3d_{Ti}$ HOMO-to-LUMO promotion. This orbital assignment is corroborated by spectroscopic evidence, photoelectron spectroscopy (PES),[25] and detailed quantum chemical calculations (vide infra). [Note: The PES studies show that the HOMO is a π-orbital located on the NCS^- ligands.] It has been reported that the lowest energy absorption band shifts to higher energy in increasingly polar solvents and increasingly rigid substrates.[26,27] This is a good indication that the lowest energy singlet is charge transfer in nature as well.

(B) Lifetimes. The phosphorescence lifetimes in a PMMA plastic film and in an organic glass are listed in Table 1. Each decay curve was fit to a single exponential over five lifetimes. Of particular interest is the observation that the 77 K phosphorescence lifetime (excited with a <10 μJ 532 nm laser pulse) in the organic glass is 653 μs, nearly 1.8 times longer than the 373 μs lifetime observed at 77 K in a PMMA plastic; this is fully addressed in the discussion section of this article. The excitation conditions for the TRIR experiments are rather severe (1 mJ laser pulses) and local heating will certainly be an issue under these conditions. To address this issue, we performed the lifetime experiments at several excitation powers from 1 μJ to 1 mJ. In PMMA, the luminescence lifetime decreased continually from 374 μs at low excitation powers to 79.4 μs at high excitation powers, whereas only a modest decrease in lifetime from 653 μs to 589 μs in the $CHCl_3$:CCl_4:CH_2Cl_2 glass was observed. These experiments have revealed that at high excitation powers significant local heating in PMMA samples occurs, whereas only modest local heating in glass samples was observed. We can quantify the rise in temperature caused by the laser pulse by measuring the luminescence lifetimes at temperatures above 77 K. A luminescence lifetime of 79.4 μs in PMMA corresponds to a temperature of 103 K while a luminescence lifetime of 589 μs in a 3:2:1 $CHCl_3$:CCl_4:CH_2Cl_2 glass corresponds to a temperature of 82.5 K. One can see that the local heating can be severe in plastic samples while laser induced heating is modest in glass samples under the conditions of the TRIR experiments (vide infra). Such local heating effects can conceivably complicate TRIR spectra in which even small effects can also show up. We have addressed this issue in detail below.

(C) Infrared Spectra. Ground-state IR spectra, in the CN stretching region, of $(Cp)_2Ti(NCS)_2$ in PMMA and $CHCl_3$:CCl_4:CH_2Cl_2 at 77 K are depicted in Figures 3a and 4a. The IR spectra in the two media are nearly identical and display two bands in the CN stretching region. The higher frequency band is assigned to the symmetric CN stretch of the two isothiocyanato groups on the molecule (the symmetry is A in the C_2 point group). The lower frequency vibration is assigned to the antisymmetric CN stretch of the two isothiocyanato groups (the symmetry is B under the C_2 point group). These assignments are based upon quantum chemical studies (see Table 2). The only difference is that in the PMMA IR spectrum, the two CN stretching bands are shifted to slightly lower frequencies ($\Delta\nu_{anti} = 17$ cm^{-1} and $\Delta\nu_{sym} = 23$ cm^{-1}) than what is measured in the organic glass spectrum.

(D) Excited-State Infrared Signatures. The dynamic TRIR data are collected through the AC-coupled output of the MCT detector. Because of this, the AC spectrum only records IR signatures that change in response to the applied laser excitation, which is in turn synchronized to the digital storage oscilloscope (static IR absorptions are silent). Therefore, the raw data can be interpreted in terms of a *change* in optical density vs time (note: in the raw data, the change in optical density is proportional to AC volts). The TRIR spectra (after conversion to ΔA) are displayed in Figures 3b and 4b. Both spectra are similar in band shape with two bleaches corresponding, in frequency, to the symmetric and antisymmetric CN stretches of the isothiocyanato ligands of the ground state $(Cp)_2Ti(NCS)_2$ molecule. Also, two new IR bands grow in, both in the CN stretching region, with positive intensities and energies shifted to slightly lower frequencies, as compared to the symmetric and antisymmetric CN stretching bands in the ground-state IR spectrum.

(25) Guimon, C.; Pfister-Guillouzo, G.; Besancon, J.; Meunier, P. *J. Chem. Soc., Dalton Trans.* **1987**, *1*, 107−110.
(26) Al-Alousy, A.; Burgess, J.; Samotus, A.; Szklarzewicz, J. *Spectrochim. Acta* **1991**, *47 A*, 985−989.
(27) Burgess, J.; Maguire, S.; McGranaghan, A.; Parsons, S. A.; Nowicka, B.; Samotus, A. *Trans. Metal Chem.* **1998**, *23*, 615−618.

Table 2. Experimental and Predicted Ground and Excited State Frequencies[a]

frequency	experimental PMMA	experimental glass	b3LYP/6–31g*	hf/6–31g**	hf/6–31g*	hf/3–21g
$\nu_{Sym}^{g.s.}$	2055 (0.60)	2072 (0.71)	2035 (0.42)	2092 (0.61)	2078 (0.61)	2121 (0.66)
$\nu_{Anti}^{g.s.}$	2015 (1.00)	2038 (1.00)	2000 (1.00)	2052 (1.00)	2038 (1.00)	2086 (1.00)
$\nu_{Sym}^{e.s.}$	2049 (0.89)	2059 (0.45)	N/A	2064 (0.50)	2050 (0.50)	2090 (0.55)
$\nu_{Anti}^{e.s.}$	1996 (1.00)	2013 (1.00)	N/A	1996 (1.00)	1982 (1.00)	2031 (1.00)

[a] Relative intensities are in parentheses. The relative intensities were calculated from individual spectra or calculations.

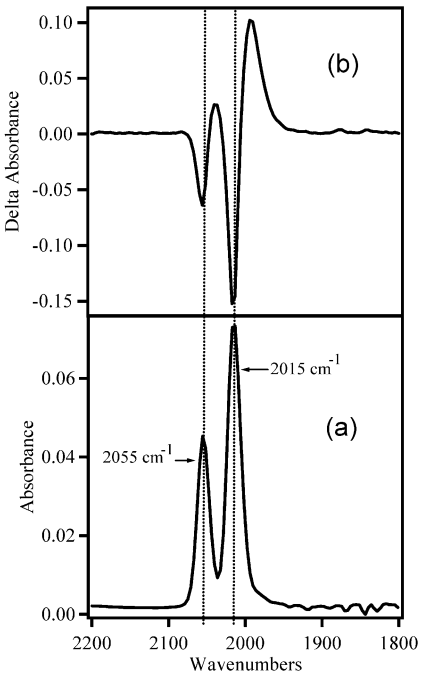

Figure 3. $(Cp)_2Ti(NCS)_2$ in PMMA plastic at 77 K: (a) ground-state FTIR (from spin coated films on CaF_2 optical flats), (b) TRIR spectrum, 5 μs time slice, 532 nm laser excitation, 1 mJ laser pulse, 4 ns pulse width.

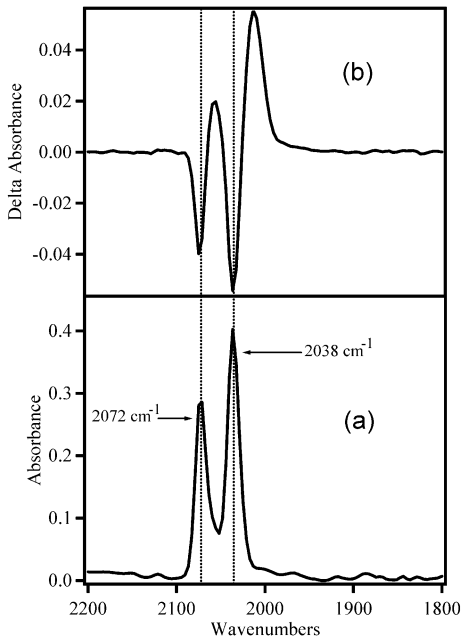

Figure 4. $(Cp)_2Ti(NCS)_2$ in organic glass at 77 K: (a) ground-state FTIR, (b) TRIR spectrum, 50 μs time slice, 532 nm laser excitation, 1 mJ laser pulse, 4 ns pulse width.

Because the TRIR data contain both the grow-in of the excited state FTIR spectrum and the bleach of the ground state FTIR spectrum, the excited state spectra were derived from the initial time slices of the TRIR data and the ground state FTIR spectra in which the ground state spectra are simply added back into the TRIR data (i.e., subtracting out the ground state bleach). The resultant excited state IR spectra are depicted in Figures 5 and 6 where the dotted lines are the ground state spectra and the solid lines are the excited state spectra. One can see that the excited state IR spectra are remarkably similar to their ground-state counterparts but differ in two important respects. They are shifted to lower frequencies ($\Delta\nu_{sym}^{PMMA} = 6$ cm^{-1}, $\Delta\nu_{anti}^{PMMA} = 19$ cm^{-1}, $\Delta\nu_{sym}^{glass} = 13$ cm^{-1}, $\Delta\nu_{anti}^{glass} = 25$ cm^{-1}) and are broadened (only slightly in the glass samples but considerably so in the case of PMMA). This broadening is most certainly due to the same local heating effect that we have observed in the luminescence lifetime studies and is discussed fully below.

Depicted in Figures 7 and 8 are the time progressions of the TRIR signatures in PMMA and the organic glass, respectively. The time evolution of the PMMA study is divided into twenty-five 5-μs time slices, whereas the organic glass study is composed of twenty 50 μs time slices. Clearly, the decay process of $(Cp)_2Ti(NCS)_2$ in an organic glass is much longer than that observed for samples dissolved in PMMA plastics. To explore the time evolution of the TRIR spectra, the data have been

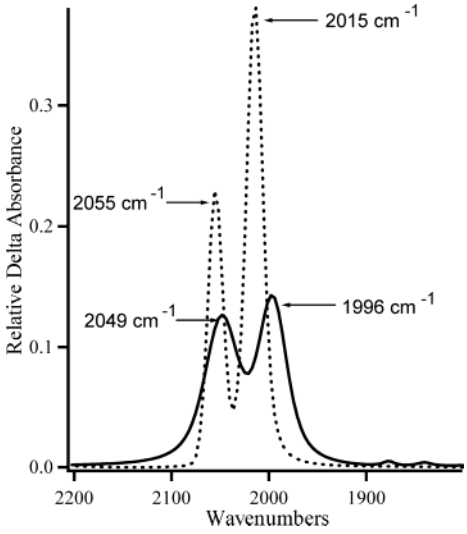

Figure 5. Deconvolution of TRIR data and ground-state FTIR data at 77 K and in PMMA plastic (····· ground-state IR spectrum, — excited-state IR spectrum).

analyzed with the technique of singular value decomposition (SVD). This was done to determine the number of temporally distinct IR signatures that exist in the time-resolved data sets (basis spectra) and to extract the time dependence of each of those eigenvectors (propagation vectors). SVD has been exploited by a number of researchers for analyzing time-dependent

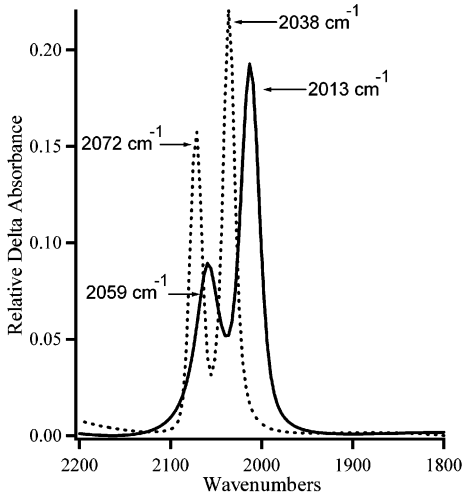

Figure 6. Deconvolution of TRIR data and ground-state FTIR data at 77 K and in organic glass (····· ground-state IR spectrum, — excited-state IR spectrum).

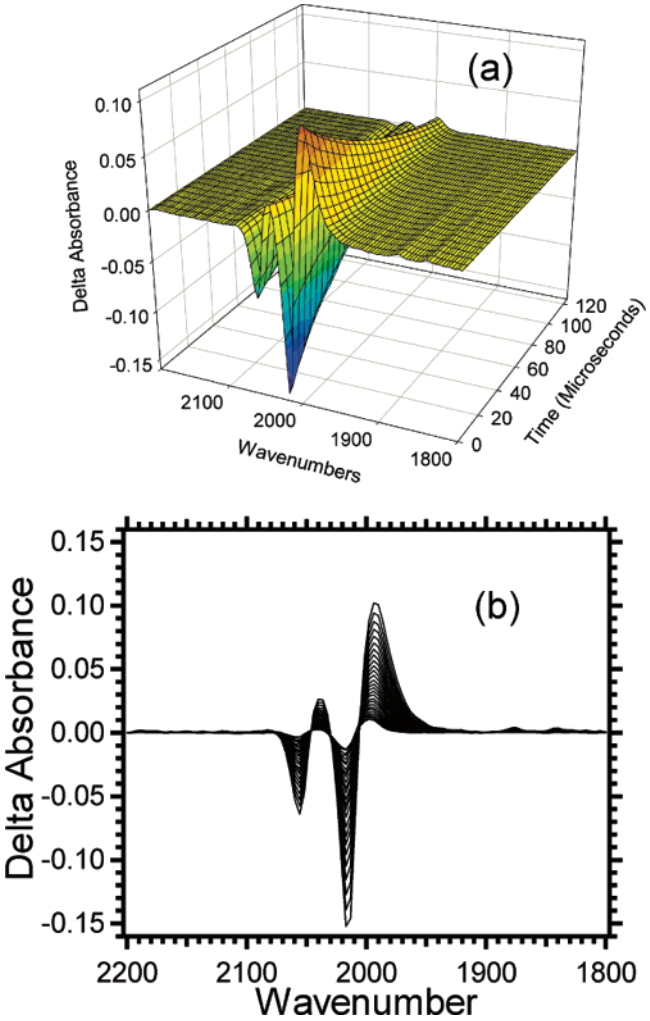

Figure 7. TRIR spectra of $(Cp)_2Ti(NCS)_2$ in PMMA at 77 K. Laser excitation is 532 nm, 1 mJ/pulse, 10 Hz repetition rate, and 4 ns pulse width. Each time slice is 5 μs. (a) Time vs wavenumber vs ΔA. (b) Time slice overlay.

spectroscopic data and the details of the present analysis are presented in the Supporting Information accompanying this article.[28−31]

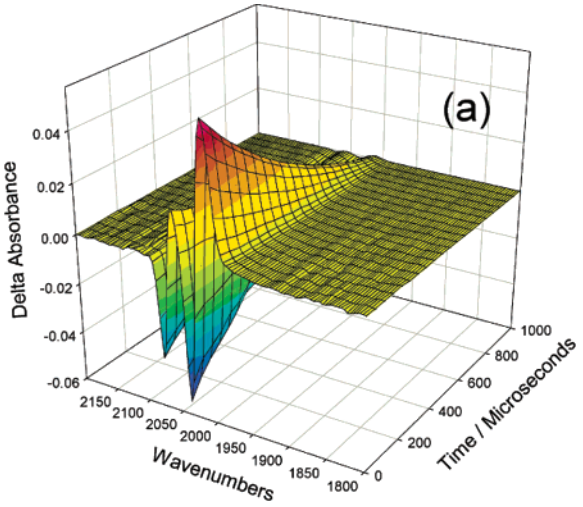

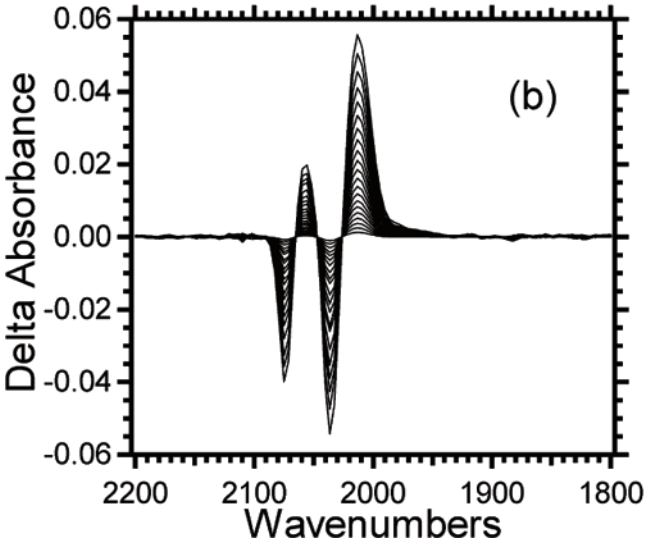

Figure 8. TRIR spectra of $(Cp)_2Ti(NCS)_2$ in $CHCl_3$:CCl_4:CH_2Cl_2 glass at 77 K. Laser excitation is 532 nm, 1 mJ/pulse, 10 Hz repetition rate, and 4 ns pulse width. Each time slice is 50 μs. (a) Time vs wavenumber vs ΔA. (b) Time slice overlay.

The results of the SVD analyses reveal a trivial solution in that each TRIR data set contains a single eigenvector and the time propagation of that vector matches the luminescence lifetime of the phosphorescence band when measured under identical experimental conditions. This is conclusive evidence that the TRIR experiment is indeed measuring the same excited state manifold as probed by the luminescence experiments (i.e., the lowest energy vibrationally relaxed ^{3}LMCT manifold) in accordance with the Crosby−Kasha rule.[32] The lifetimes extracted from the SVD analysis are recorded in Table 1.

(E) MO Diagrams. Reported are the results of HF−SCF and DFT−SCF studies for the determination of molecular wave functions and MO diagrams for $(Cp)_2Ti(NCS)_2$. Shown in Figure 9 is a summary of a DFT study using the hybrid functional B3LYP and the 6-31G split basis set. The MO diagram is in

(28) Golub, G. H.; Reinsch, C. *Numer. Math.* **1970**, *14*, 403−420.
(29) Nagle, J. F.; Parodi, L. A.; Lozier, R. H. *Biophys. Soc.* **1982**, *38*, 161−174.
(30) Hofrichter, J.; Henry, E. R.; Sommer, J. H.; Deutch, R.; Ikeda-Saito, M.; Yonetani, T.; Eaton, W. *Biochemistry* **1985**, *24*, 2667−2679.
(31) Hug, S. J.; Lewis, J. W.; Einterz, C. M.; Thorgeirsson, T. E.; Kliger, D. S. *Biochemistry* **1990**, *29*, 1475−1485.
(32) Demas, J. N.; Crosby, G. A. *J. Am. Chem. Soc.* **1970**, *92*, 7262−7270.

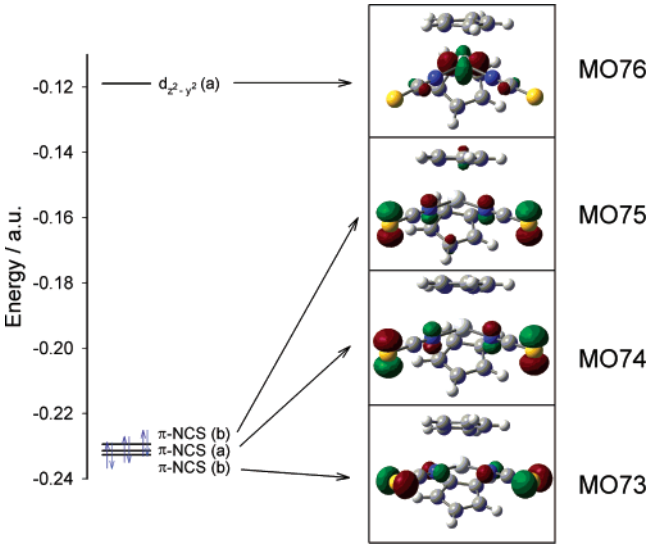

Figure 9. MO diagram for $(Cp)_2Ti(NCS)_2$ based upon the results of a DFT calculation utilizing the B3LYP functional and 6−31g split basis. Please note that the labels on the d-orbitals reflect the choice of axis labels in Figure 1 (example: $3d_{z^2-y^2}$ is usually written as $3d_{x^2-y^2}$).

agreement with PES studies on $(Cp)_2Ti(NCS)_2$ which clearly show that the HOMO is indeed a π-orbital located in the NCS^- ligands.[25] Other DFT calculations using the same functional but different basis functions (3-21G, 6−31 g* and LANL2DZ) yield very similar LCAO-MOs and identical orderings for the highest five occupied and lowest five unoccupied MOs. Similar calculations using the HF method yielded similar results except that the ordering between MO 73 and 74 and between MO 79 and 80 have been switched (see Figure 9). This is not surprising in that the Fock operator does not attempt to correlate each electron's motion but rather calculates the exact repulsion between effective charge distributions representing each electron's spatial occupation (HF neglects so-called "Coulomb-holes"). This lack of electron correlation can lead to severe errors in electronic energies and MO ordering. Therefore if one wishes to use the results of HF calculations to model other molecular properties it is always a good idea to compare those results with a method that can treat electron correlation. DFT is one such method in which the minimum energy of a system is found by parametrically varying the electron density and thus electron correlation is intrinsic. Therefore, if an appropriate functional is chosen, DFT will normally give more accurate energies and energy spacings between MOs. Regardless, it is reassuring that the LCAO−MOs and their ordering are in good general agreement between different computational methods and choices of basis.

The lowest five unoccupied MOs comprise the complete set of 3d orbitals localized on the Ti metal center. One also sees that the LUMO, the $3d_{z^2-y^2}$ Ti orbital, is significantly lower in energy than the rest of the 3d orbitals and will be the acceptor orbital most directly involved in the lowest energy charge transfer (CT) transitions. On the other hand the three highest occupied MOs are all very close in energy and very similar in nature. Each MO is a π-orbital located on the isothiocyanato ligands of the molecule and has a node located on the carbon atoms making it a nonbonding MO in the nearest neighbor sense but is slightly bonding in overall character. These π-orbitals are either oriented in the π plane (MO 74 and 75; Figure 9) or in the σ plane (MO 73; Figure 9) of the molecule. The π-plane is defined as the *yz*-plane in Figure 1 and the σ-plane is defined as the *xz*-plane in Figure 1. A more detailed MO diagram can be found in the Supporting Information (Figure S4).

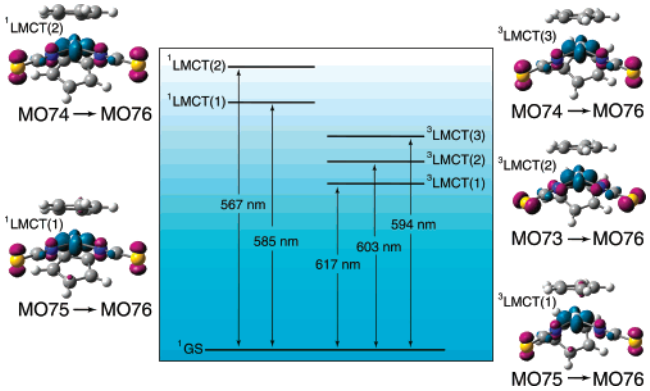

Figure 10. Jablonski diagram for $(Cp)_2Ti(NCS)_2$ based upon the results of a TD-DFT calculation utilizing the B3LYP functional and the 6−31g split basis. The pictures on either side of the Jablonski diagram are electron density difference maps (EDDM). Blue/red = increased/decreased electron density relative to ground state.

(F) State Diagrams. At the simplest conceptual level, electronic excitation involves the promotion of a single electron from an occupied MO (normally the HOMO) to an unoccupied MO (normally the LUMO). Therefore, by simple inspection of the MO diagram (Figure 9) one can describe the lowest excited singlet and triplet states as a ligand-to-metal charge transfer (LMCT) from the isothiocyanato ligand into the Ti(IV) metal center. Unfortunately, this simple method is not always very accurate for molecules with many close-lying states. Therefore the current study capitalizes on two independent excited-state models in developing a more accurate state diagram for $(Cp)_2Ti(NCS)_2$.

Studies using both CIS and TD−DFT have predicted that the lowest two singlet states are ^{1}LMCT ($\pi_{NCS} \rightarrow d_{z^2-y^2}$) and the lowest 3 triplet states are also ^{3}LMCT ($\pi_{NCS} \rightarrow d_{z^2-y^2}$) in $(Cp)_2Ti(NCS)_2$. This leads to an important verification that excited state frequency calculations, which are based upon the HF method, do indeed model the correct excited states (in an orbital sense), or a very close facsimile. Even though both methods have lead to the same qualitative state diagram, TD−DFT yielded energy gaps between ground and excited states that are more quantitatively consistent with experimentally observed absorption and phosphorescence bands (CIS energy gaps were all considerably higher in energy than experimental values). Depicted in Figure 10 is a Jablonski diagram constructed from the results of a TD−DFT calculation that utilized the B3LYP functional and the 6-31G split basis. The pictures to the left and right of the diagram are electron density difference maps (EDDM) for each state depicted in the state diagram. EDDM's pictorially describe the change in the spatial distribution of electron density associated with excitation from one state to another.

For the EDDM's in Figure 10, the regions depicted in red represent decreased electron density compared with the ground state and the regions depicted in blue represent increased electron density compared with the ground state. This analysis predicts three close lying triplet manifolds within 628 cm^{-1} of one another (the lowest two are separated by only 337 cm^{-1}). It is worth noting that this is larger than the observed ~100 cm^{-1} shift between organic glass and PMMA samples seen in

the phosphorescence spectra but higher lying states are thermally accessible at 77 K and above. The energy gap between the lowest triplet state and the ground state is a good estimate of the Franck−Condon transition (i.e. the vertical excitation energy). In the absence of a direct spin forbidden $^1GS \rightarrow {}^3LMCT$ absorption measurement, the Franck−Condon transition can be estimated by taking the difference between the 0−0 luminescence transition (band origin) and the luminescence peak and adding that difference back to the back to the 0−0 luminescence transition (this assumes that the luminescence and $^1GS \rightarrow {}^3LMCT$ absorption bands are mirror images of another; which is normally the case). The vibrational fine structure in the luminescence spectrum of single crystals of $(Cp)_2Ti(NCS)_2$ is well resolved at 2.7 K and the 0−0 transition wavelength is measured to be 641 nm, whereas the maximum vibrational-electronic transition is at 665 nm (this is the 0−3 transition).[33] Therefore, the estimated Franck−Condon transition is ~575 nm. The calculated transition wavelength of 617 nm is in reasonable agreement with that estimated from the luminescence data considering the level of theory used for these studies and the fact that the luminescence data can only give an estimate of the Franck−Condon transition.

(G) Simulated Ground and Excited-State Infrared Spectra. The vibrational studies presented in the current body of work only probe the IR frequencies and intensities in the ground electronic state (FTIR) and the lowest vibrationally relaxed triplet state (TRIR). Therefore, the present work only calculates IR spectra for these two states. The calculated ground-state frequencies and intensities are in good agreement with those experimentally measured, especially between the calculations using either the 6−31g* or 6−31g** basis sets and the IR spectra in the 3:2:1: $CHCl_3$:CCl_4:CH_2Cl_2 glass (see Table 2). The calculated excited state frequencies and intensities are also in reasonable agreement with experiment. Even through the experimental excited state frequencies are reasonably modeled with the CIS method, it is clear that the calculated excited-state frequency shifts are a factor of 2 larger than experimentally observed. The largest factor contributing to this error is that the modeling study ignores the geometric relaxation in the excited state and simply uses the ground state geometry in calculating the excited state frequencies. This is a gross approximation as indicated experimentally by the broad structureless luminescence spectra at 77 K. In each case, the excited state frequencies are shifted to slightly lower energies and the relative intensities in both the ground and excited states are such that the antisymmetric CN stretch (on the NCS^- ligands) is always more intense than the symmetric stretch, just as is seen in the FTIR and TRIR spectra (see Figures 6 and 7).

IV. Discussion

(A) State Assignment. From the relatively long lifetimes (in 10^2 μs range at 77 K) and large Stokes shifts of $(Cp)_2Ti(NCS)_2$ in both PMMA and the $CHCl_3$:CCl_4:CH_2Cl_2 77 K glass, it is clear that the spin parity of the lowest emitting excited state is a triplet. This is consistent with state assignments previously made for other similar $(Cp)_2TiX_2$ compounds.[1] Quantum chemical studies as well as previous studies using photoelectron spectroscopy[25] have revealed that the lowest occupied molecular orbitals are a set of close lying symmetry adapted π-molecular orbitals located on the isothiocyanato ligands. Each of these MO's is effectively nonbonding in that there is a node on the carbon atom separating the nitrogen and sulfur atoms of the isothiocyanato ligands. The lowest five unoccupied orbitals are the d-orbitals located on the Ti metal, with the $d_{z^2-y^2}$ orbital being the lowest and well separated in energy from the rest of the d-set. Therefore the transition that gives rise to the observed luminescence is a spin forbidden $^3LMCT \rightarrow {}^1GS$ transition with the NCS^- ligands being reduced and the metal being oxidized. This state assignment is successfully modeled using both CIS and TD−DFT. EDDM's derived from excited state (CIS or TD−DFT) calculations and the corresponding ground-state calculations reveal that the lowest triplet state is indeed a ^3LMCT originating from the orbital promotion of an electron from a π-orbital on the isothiocyanoto ligands and oriented in the π plane of the molecule to the $d_{z^2-y^2}$ orbital on the Ti. This is exactly what is predicted for the promotion of an electron from the HOMO into the LUMO as arrived at from the molecular orbital diagrams. This assignment is entirely consistent with the experimental results.

As noted above we have observed a notable decrease in quantum efficiency and a concomitant decrease in luminescence lifetime for samples dissolved in PMMA plastics in comparison to samples embedded in 3:2:1 $CHCl_3$:CCl_4:CH_2Cl_2 77 K glasses. We have also observed a significant temperature dependence to the luminescence lifetimes as well as some broadening of the excited-state IR spectra. Theoretical studies have shown that two triplet manifolds lie within 377 and 628 cm^{-1} of the lowest triplet manifold. Moreover, the degeneracy of each triplet manifold will be lifted by spin−orbit coupling yielding nine excited states in very close proximity to one another. At 77 K and above, these states are all thermally accessible and it is quite likely that the luminescence actually originates from a weighted average of all nine states according to Boltzmann's statistics (Note: Boltzmann equilibrium implies that the equilibrated excited states will decay with a *single temperature dependent* lifetime that is a weighted average of the transient decays from each individual state). Although state crossing is unlikely given the degree of solvatochromic shift, the relative energy separation between states can change subtly between plastic and glass samples and this can lead to significant changes in both luminescence intensities (i.e., quantum efficiencies) and luminescence lifetimes. Moreover, such a model can also account for the dramatic temperature dependence of the luminescence lifetimes (simple Boltzmann statistics) and even the apparent broadening of the excited-state IR spectra in comparison to the ground-state IR spectra. The broadening of the excited-state IR spectra would be expected from an excited-state manifold of nine distinct states all with a similar orbital nature. It should also be noted that all nine close lying excited states are ^3LMCT in nature and are derived from essentially the same orbital parentages. Therefore, this model does not invalidate the state assignment for the lowest energy transition ($^3LMCT \rightarrow {}^1GS$ in nature).

(B) TRIR Studies. The present study is unique in that it is the first TRIR study to spectroscopically probe a ^3LMCT manifold and the first to be conducted in a 77 K organic glass and PMMA plastic. Conducting the TRIR experiments at 77 K has, in part, lead to the unusually clean TRIR spectra presented

(33) Meyer, G. D.; Ortiz, T. P.; Costello, A. L.; Brozik, J. A.; Kenney, J. W. III *Rev. Sci. Instrum.* **2002**, *73*, 4369−4374.

above. By cooling the samples to 77 K nonradiative processes are turned off or slowed. This has led to longer lifetimes and smaller thermal pulses. The longer lifetimes are particularly advantageous in that the limited IR flux of the probe can be integrated over a longer time interval and thus yield larger signals in comparison to faster decaying transients. We have observed some local heating however and this has led to a shortening of the TRIR transients (for the reasons described above) but this shortening is concomitant with an identical shortening of the luminescence lifetimes when measured under identical experimental conditions. These effects are slight for glass samples but are significant in PMMA plastic samples. Moreover, the experimentally observed TRIR signatures of both glass and plastic samples are nearly identical with regard to shifts of the in the excited-state spectra in comparison to the ground-state spectra. The major difference is that the excited-state IR spectrum in the plastic sample is broadened in comparison with the excited-state IR spectrum for the glass, but this is also consistent with the arguments presented above. Because of the correlation between luminescence lifetimes and TRIR transients we can be confident that the TRIR is still probing the lowest emitting triplet manifold regardless of the local heating.

From the quantum chemical studies (and from other studies with similar ligands; most notably the isotopically labled $^{15}NCS^-$, $N^{13}CS^-$, and $^{15}N^{13}CS^-$ ligands; see Supporting Information Figure S5), we have assigned the two bands occurring between 2100 and 2000 cm^{-1} in the FTIR spectra to the symmetry adapted symmetric and antisymmetric CN stretches on the NCS^- ligands. Of particular importance is that the TRIR data have revealed excited state IR spectra that are essentially the same as the ground state spectra but shifted slightly to lower frequencies. This is exactly what one would expect from an excited state that was derived from the orbital promotion of an electron from a delocalized symmetry adapted slightly bonding π orbital (formally nonbonding in the nearest neighbor sense; Figure 9) on the NCS^- ligands to the metal $d_{z^2-y^2}$ orbital. [The authors would like to note the subtle language used in describing the HOMO. We have been referring to the HOMO as nonbonding because of the node located on the carbon separating the N and S atoms on the NCS^- ligands, but the overall SCF bond order is slightly bonding.] Moreover, the ground-state IR spectra and the excited-state IR spectra in the CN region of $(Cp)_2Ti(NCS)_2$ are very similar with respect to the relative spacing between ν_{sym} and ν_{anti} stretches and the relative intensities between these two bands. This strongly suggests that the C_2 symmetry is retained in the excited state; i.e., the HOMO is a delocalized nonbonding NCS^- π orbital. If the ^{3}LMCT manifold of $(Cp)_2Ti(NCS)_2$ were to involve excited-state symmetry breaking, one would not expect this level of similarity to be preserved between ground and excited-state spectra. The quantum mechanical modeling of the excited state, which uses strict C_2 symmetry and reproduces the excited state spectra reasonably well, backs up this conclusion. In an attempt to estimated the frequency shift for a localized ^{3}LMCT (π_{NCS^-}) $\rightarrow$ $d_{z^2-y^2}$) excited-state we have modeled the hypothetical molecules $(Cp)_2Ti(NCS)(H)$ and $(Cp)_2Ti(NCS)(F)$ in the same manner as $(Cp)_2Ti(NCS)_2$ and have shown that for a localized $\pi_{NCS^-} \rightarrow d_{z^2-y^2}$ orbital promotion the expected transient IR shifts are in the range of 140 cm^{-1}. This is much larger than shifts we observe experimentally. Moreover, if we perform a frequency calculation on an excited-state derived from a $\pi_{Cp} \rightarrow d_{z^2-y^2}$ orbital promotion, we find very little change associated with the CN stretch.

Does the apparent symmetry preservation in the ^{3}LMCT state of $(Cp)_2Ti(NCS)_2$ generally hold true in other molecules with ^{3}LMCT excited states or is $(Cp)_2Ti(NCS)_2$ a special case? Moreover, is the nonbonding nature of the HOMO reason enough to preserve the symmetry in the excited-state rather than the direction of the charge transfer (LMCT vs MLCT)? The answers to these questions must await the identification and investigation of broader classes of molecules with ^{3}LMCT excited states and further CT studies involving nonbonding MO's.

Acknowledgment. The authors would like to acknowledge the NSF REU program at the University of New Mexico for the support of the undergraduate researchers on this project; all of the authors, with the exception of J.A.M., J.A.B., and J.W.K, were undergraduates while working on this project. The University of New Mexico, Eastern New Mexico University (where J.W.K and M.A.S. originated this work), and Concordia University—Irvine are thanked for financial and programmatic support. It is a pleasure to acknowledge Ms. Alison Costello for developing a number of new organic glasses, one of which was employed in the current study. Professor Tom Niemczyk and Mr. Anding Zhang deserve acknowledgment for helpful discussions regarding SVD analysis (multivariate analysis). J.W.K and M.A.S. wish to thank Professor Gregory Gellene for his assistance with critically important preliminary quantum chemical calculations on titanium metallocene systems.

Supporting Information Available: Detailed schematic diagram of the experimental setup, calculated results and a comparison to a variety of experimentally observed (X-ray data) bond angles and lengths (Table S1), details of the present analysis of SV, detailed MO diagram (Figure S4), and information about other studies with similar ligands; most notably the isotopically labeled $^{15}NCS^-$, $N^{13}CS^-$, and $^{15}N^{13}CS^-$ ligands (Figure S5) This material is available free of charge via the Internet at http://pubs.acs.org.

JA028769U